RSC Advances

ROYAL SOCIETY OF CHEMISTRY

www.rsc.org/advances

Preparation of Silver Nanoparticles Supported Mesoporous Silica Microspheres

with Perpendicularly Aligned Mesopore Channels and Their Antibacterial

Activity

Ren-Shu Huang[a], Bao-Fei Hou[b], Hai-Tao Li[b], Xu-Cheng Fu[b][*] and Cheng-Gen Xie[b]

[a] Chemistry and Life Science Department, West Anhui University, Lu'an, Anhui

237015, PR China

[b] Anhui Provincial Laboratory of Biomimetic Sensor and Detecting Technology, West

Anhui University, Lu'an, Anhui 237015, PR China

[*]Author to whom all correspondence should be addressed

E-mail: fxc8307@wxc.edu.cn (X.-C.Fu)

Tel.: +86 (0) 5643305690

Fax.: +86 (0) 5643305660

ABSTRACT

In this study, a facile and an effective route for the preparation of silver nanoparticles supported surface mesoporous silica microspheres with perpendicularly aligned mesopore channels was reported. The surface mesoporous silica microspheres (mSiO$_2$) were synthesized by a sol-gel method. The mSiO$_2$ then were functionalized with 3-aminopropyltriethoxysilane (APTS) to provide amino functional groups for the absorption of Ag$^+$. Silver nanoparticles were directly created on the surface of mSiO$_2$ by in stiu chemical reduction of Ag precursor using ultrasonic wave reaction method. The prepared silver nanoparticle supported surface mesoporous silica nanocomposites (mSiO$_2$@NH$_2$@Ag) were characterized with FT-IR, X-ray Photoelectron Spectroscopy, X-ray diffraction, scanning electron microscope and high-resolution transmission electron microscopy. Antibacterial activities of the synthesized mSiO$_2$@NH$_2$@Ag were investigated against Gram-negative Escherichia coli (E. coli) and Gram-positive Staphyloccocus aureus (SAU) using the conventional plate-count method. The results demonstrated that the synthesized nanocomposites exhibited excellent antibacterial properties against E. coli and SAU. Furthermore, because the slow release property of silver, the synthesized nanocomposites can be used as an economic recyclable material in various antibacterial applications, such as water purification systems and environmental control of bacteria.

1. Introduction

Infection with the bacteria is a global problem concerning the public security and health[1-3]. Many approaches have been discussed to deal with bacteria's antibiotic resistant problem and many antibacterial agents, especially some inorganic nanoparticles[4], e.g. gold[5], titanium[6, 7], copper[8], magnesium oxide[9] and zinc oxide[10, 11] and silver[2, 12-14] have been used to reduce the risk of people's health[15-17]. Significant studies indicated that silver nanoparticles have strong antibacterial effects because of its higher antibacterial activity and broad antibacterial spectrum even at low concentrations [18-20], and relatively nontoxic to human cells. Furthermore, silver nanoparticles could be easily embedded within inorganic substrates and these silver nanoparticles containing materials are capable of slow release of silver over an extended period, which is superior, in the aspects of safety, stabilities and longtime antibacterial activities, to those conventional organic antibacterial materials[21]. At present, zeolite[22, 23], clay[24], calcium phosphate[25], silica[26] and mesoporous materials[27-32] have been reported as supports for fabricating silver-containing antibacterial agents. However, the limitation of these silver-containing antibacterial materials is that most silver nanoparticles were doped in the inner substrates and the inner silver nanoparticles may not contribute to the antibacterial effect at all. Surface mesoporous silica material with mesopore channels perpendicular to the core surface is expected to be a good candidate for idea inorganic substrates owing to its unique perpendicular orientation mesoporous channels structures and large surface area[33-35]. These open perpendicular mesoporous channels could conveniently dope high dense

silver nanoparticles at the outer channels and improve the antibacterial efficiency. However, there was little report about the surface mesoporous silica material based silver nanoparticles for antibacterial applications.

In this study, we have developed an effective route to prepare silver nanoparticles-supported surface mesoporous silica nanocomposites for antibacterial applications. First, we fabricated core-shell structured surface mesoporous microspheres with SiO_2 particles cores and perpendicularly aligned mesoporous silica shells (mSiO$_2$). Then, 3-aminopropyltriethoxysilane (APTS) was modified onto the mSiO$_2$ to graft amino functional groups onto the surface mesopore channels (mSiO$_2$@NH$_2$). The amino groups of APTS on the surface of mesopore channels provided the active site for the absorption of Ag$^+$ through complexation interaction and increased the loading amount of silver ions on the mSiO$_2$. The silver nanoparticles were directly created on the surface of mSiO$_2$ by in stiu chemical reduction of Ag precursor using ultrasonic wave reaction method. The synthesized silver nanoparticle supported mesoporous silica (mSiO$_2$@NH$_2$@Ag) was examined against Gram-negative Escherichia coli (E. coli) and Gram-positive Staphyloccocus aureus (SAU) for their antibacterial efficacy.

2. Experimental

2.1. Reagents

Tetraethoxysilane (TEOS), anhydrous ethanol, ammonium hydroxide (25 wt% NH$_3$ in water), and stearyltrimethyl ammonium bromide (STAB) were obtained from Beijing Chemical Company. AgNO$_3$ and 3-aminopropyltriethoxysilane (APTS)

purchased from Sigma-Aldrich and used as supplied. All other reagents were commercially available as analytical reagent grade

2.2. Preparation of $mSiO_2@NH_2$ microspheres

The core-shell $mSiO_2$ microspheres were synthesized according to our previous work[35, 36]. Briefly, 0.2 g SiO_2 (~130 nm) particles were dispersed in mixed solution containing of STAB (0.67 g, 1.78 mmol), concentrated ammonia aqueous solution (0.6 mL, 28 wt.%), deioned water (60 mL) and ethanol (30 mL). The mixed solution was stirred for 0.5 h and then 1.1 mL distilled TEOS was added. After the reaction for 12 h at room temperature, the suspension was centrifuged and washed with ethanol. The obtained white precipitate was vacuum dried at 343 K overnight and then was further calcined at 823 K for 6 h in air in order to remove STAB from the composites. 0.1 g of as-synthesized $mSiO_2$ microspheres and 1 mL of APTS were added into anhydrous toluene to make 50 mL of mixture solution. The mixture was refluxed for 18 h under dry nitrogen. The resulting $mSiO_2@NH_2$ microspheres were separated by centrifuge, washed with toluene, ethanol and water in turn, and then vacuum dried at 343 K overnight for use.

2.3. Preparation of $mSiO_2@NH_2@Ag$

1.0 g of the as-prepared $mSiO_2@NH_2$ microspheres was suspended in a series of 60 mL $AgNO_3$ aqueous solution with different concentrations (0.5, 1.0, 2.0, 2.5, 3.0 M) in brown bottles and the mixed solution was ultrasonic treated for 2 h under dark condition, then was stirred at 313K for another 2 hours. The silver (I) ions were reduced to silver nanoparticles on the mesopore channels of $mSiO_2@NH_2$ surface.

The precipitate was separated by filtration and washed with deionized water to remove $AgNO_3$ on the external surface. Finally, the composites were dried in vacuum at 343K for 12 h obtained gray-colored $mSiO_2@NH_2@Ag$ nanocomposites. The $mSiO_2@Ag$ without APTS modification procedure was prepared by the same procedure above and used for control antibacterial activity experiment.

2.4. Experimental measurement method

The transmission electron microscopy (TEM) images were obtained on the JEOL-2010 transmission electron microscope at an accelerating voltage of 200 Kv. The scanning electron microscopy (SEM) images were taken by using a field-emission scanning electron microscopy (FESEM, JEOL JSM-6700F, 10 Kv). X-ray powder diffraction (XRD) pattern of the products was recorded on a D/max 2550 X-ray Diffractometer (RigaKu, Japan) using Cu Kα radiation ($\lambda = 1.54178$ Å). The FT-IR spectra in KBr were recorded using a Perkin-Elmer spectrometer (model GX2000). XPS analysis was carried out using a Thermo ESCALAB 250 equipped with a monochromatic microspot X-ray beam originating from the Al anode (Kα, X-ray at 1486.6 eV) with a spot diameter of 500μM. The data were recorded at room temperature and under a pressure below 10^{-6} Pa.

2.5. Microbiological experiment

The antibacterial activities of $mSiO_2@NH_2@Ag$ were tested on E. coli as a gram negative strain and SAU as a gram positive strain. Both gram negative and gram positive bacteria were used for inhibitory zone tests, minimum inhibitory concentration (MIC) and minimum bactericidal concentration (MBC) tests to

investigate the antibacterial properties of mSiO$_2$@NH$_2$@Ag. A nutrient broth was used as the growing medium. Bacteria were grown aerobically in nutrient broth at 37 °C for 24 h.

2.5.1. Inhibitory zone tests

Nutrient agar was poured onto the petri dishes and allowed to solidify. Bacteria were spread on the plate uniformly. About 0.05 g of mSiO$_2$@NH$_2$@AgNPs were gently placed over the solidified agar gel in round shape with diameter ca. 10 mm. Plates were incubated at 37 °C for 24 h to check the zone of inhibition. The mSiO$_2$ and mSiO$_2$@Ag without APTS modification procedure were used as control and their zone of inhibition tests were tested by the same procedure for mSiO$_2$@NH$_2$@Ag.

2.5.2. MIC and MBC tests

The minimum inhibitory concentration (MIC) and minimum bactericidal concentration (MBC) against E. coli and SAU were examined by tube dilution method. The inoculation of E. coli and SAU were prepared by growing strains in Luria-Bertani (LB) liquid medium at 37 ◦C until a level of approximately 10^8-10^9 CFU/mL of bacteria were reached. A serial of doubling dilution of the mSiO$_2$@NH$_2$@Ag in the tube were prepared and each dilution was inoculated with the Luria-Bertani (LB) liquid medium in a 1:1 volume ratio, and the final concentrations of the mSiO$_2$@NH$_2$@Ag were in a range of 0.5-0.0039 mg/mL. Then, 0.2 mL of 10^9 CFU/mL E. coli or 10^8 CFU/mL SAU were added to above LB liquid medium containing different concentrations of mSiO$_2$@NH$_2$@Ag and incubated at 37 °C for 24 h with continuous agitation (180 rpm). The lowest concentration of the

mSiO$_2$@NH$_2$@Ag that inhibits the visible growth of colony formation was defined as the MIC. The MBC was determined by subculturing 0.2 mL LB liquid from broth dilution without growth of bacteria in MIC tests to LB solid medium plate. After incubation at 37 °C for 24 h, the lowest concentration of the mSiO$_2$@NH$_2$@Ag that does not support colony formation was defined as the MBC.

3. Results and discussion

3.1. Formation and characterization of mSiO$_2$@NH$_2$@Ag

The preparation of the mSiO$_2$@NH$_2$@Ag was illustrated in Fig. 1A. The core-shell structured mSiO$_2$ microspheres were produced by reacting TEOS with STAB surfactant at the surface of monodisperse SiO$_2$ particles in the presence of basic ammonia aqueous condition according our previous work [36]. The aim of the modification with amino groups onto the mSiO$_2$ microspheres was to absorb the maximum amount of Ag+ ions through the complex and electrostatic interactions between Ag+ ions and amino functional groups. Silver nanoparticles then were created by reducing Ag+ ions using ultrasonic wave reaction method. The created silver nanoparticles with high surface energy and unsaturated bonds were anchored on the surface and in the pores of mSiO$_2$@NH$_2$ by amino functional groups[29], denoted mSiO$_2$@NH$_2$@Ag. Figure 1B and C showed SEM and TEM (insert) images of mSiO$_2$. As seen in the TEM image, the ordered nanoporous SiO$_2$ layers are uniformly coated on SiO$_2$ core surface with thickness of ca. 30 nm and the nanopore channels are perpendicular to the microsphere surface. According to the result of the nitrogen adsorption-desorption isotherms analysis in our previous work [36], the BET surface

area of the prepared mSiO$_2$ here should be more than 400.0 m^2.g^{-1}. This perpendicular aligned nanoporous channels of mSiO$_2$ not only offers high surface area for the load of a larger amount of silver nanoparticles, but also could improve the antibacterial efficiency, because these open perpendicular nanoporous channels make silver nanoparticles get in touch with bacteria conveniently. The SEM and TEM (insert) images of mSiO$_2$@NH$_2$@Ag in Fig 1C showed that after the ultrasonic wave reaction process, Ag nanoparticles were loaded on the surface of the mSiO$_2$@NH$_2$ with the small sizes 4-10 nm. The ordered orientation channels in the outer layer of mSiO$_2$@NH$_2$@Ag were disappeared compared with the TEM image of mSiO$_2$ in Fig 1B, this may due to that the modification with amino groups and very small size Ag nanoparticles filled with the channels and the channels could not be distinguished.

Fig. 2A showed the FT-IR transmission spectra for the prepared mSiO$_2$, mSiO$_2$@NH$_2$ and mSiO$_2$@NH$_2$@Ag. From curve b of Fig.2, we could see that the characteristic peaks of amino groups at the region of 1382-1565 cm^{-1} and the absorbance bands of stretching vibrations of -CH$_2$ at the 2943 cm^{-1} could be observed after modification of APTS. However, these absorbance of the bands cannot observed on unmodified mSiO$_2$ microspheres (Figure 2A, curve a), which suggested that the amino functional groups has been banded with mesoporous silica surfaces[36]. Compared with curve b, we could see those different O-H stretching vibrations in 3424 cm^{-1} and the peaks of amino groups at the region of 1382-1565 cm^{-1} weakened or disappeared in curve c after silver nanoparticles loaded onto mesoporous silica surface. This was attributed to the created silver nanoparticles transformated the

terminal Si-OH groups into the Si-O-Ag network [29, 37]. The peak at 1385 cm^{-1}

corresponding to NO_3^- ion incurve c indicated that there were a certain amount of

silver ions existed in the mesopores surface[37].

The mSiO$_2$@NH$_2$@Ag also was characterized by XPS spectrum and XRD

analysis. As shown in Fig 2B, the XPS spectrum of mSiO$_2$@NH$_2$@Ag together with

that of the mSiO$_2$@NH$_2$ and mSiO$_2$ were examined. For mSiO$_2$@NH$_2$, the XPS

spectrum in the region of 392 - 410 eV of curve b showed an intense peak at 399.8 eV,

which are the characteristic peaks of N 1s in NH$_2$ groups[38]. We can conclude that the

amino functional groups have been modified onto the mesoporous silica surfaces

because that the N can only be derived from the amino functional groups. For

mSiO$_2$@NH$_2$@Ag, two bands at ca. 368.25 and 374.52 eV (Fig. 2B, insert) were

observed. These two bands were ascribed to Ag 3d$_{5/2}$ and Ag 3d$_{3/2}$ binding energies of

the metallic Ag [39, 40], which confirmed the existence of metallic Ag in our

mSiO$_2$@NH$_2$@Ag composite materials. Fig. 2C showed the room-temperature

wide-angle XRD data of mSiO$_2$@NH$_2$@Ag (curve b) and mSiO$_2$ (curve a). The

broadened diffraction peak appeared at 20-32° in both curve a and b belonging to the

amorphous porous SiO$_2$ matrix. The diffraction peaks at 38.1^{o}, 44.2^{o}, 64.7^{o} and 77.4^{o}

in curve b correspond to the (1 1 1), (2 0 0), (2 2 0) and (3 1 1) diffraction planes of

cubic silver, respectively [JCPDS No. 4-0783][30], and these appear along with a broad

peak in the 20-32° range for amorphous porous SiO$_2$. These diffraction peaks

indicated the presence of nanocrystalline Ag particles embedded on the porous SiO$_2$

matrix. The influence of the AgNO$_3$ concentrations to antibacterial activities in

preparing mSiO$_2$@NH$_2$@Ag were investigated and the results showed that the antibacterial activities remained relatively constant when AgNO$_3$ concentrations were above 2 M AgNO$_3$. This may due to that Ag loading capacity was saturated when AgNO$_3$ concentrations were more than 2 M, so we used 2 M AgNO$_3$ to prepare mSiO$_2$@NH$_2$@Ag. The calculated silver content of the mSiO$_2$@NH$_2$@Ag was ca. 3.24 wt% from the ICP-OES measurement.

3.2 The antibacterial effect test

The antibacterial effect of prepared mSiO$_2$@NH$_2$@Ag was first evaluated by inhibitory zone tests against E. coli as a gram negative strain and SAU as a gram positive strain. The inhibition zones tests of mSiO$_2$@NH$_2$@Ag, mSiO$_2$@Ag without APTS modification and mSiO$_2$ against E. coli and SAU for 24 h are shown in Fig. 3. We could see that mSiO$_2$@NH$_2$@Ag showed large inhibition zones against both SAU and E. coli. The inhibition zone diameter (IZD) of mSiO$_2$@NH$_2$@Ag against SAU was 27 cm (Fig. 3A), and the IZD against E. coli was 17 cm (Fig. 3B). However, mSiO$_2$@Ag without APTS modification procedure and mSiO$_2$ had no inhibitory effect against SAU, and only had little inhibitory effect against E. coli. The results showed that mSiO$_2$@NH$_2$@Ag exhibited good antibacterial activity and inhibited the growth of SAU and E. coli effectively due to their large inhibition zones. The mSiO$_2$@NH$_2$@Ag showed excellent antibacterial properties, whereas the mSiO$_2$ exhibited no bacterial inhibitory effects, suggesting that this antibacterial property was due to the presence of metal silver nanoparticles in the composite material. It has been reported that when the silver nanoparticles were dispersed throughout a silica

11

matrix, Ag+ ions were released when the materials interact with an aqueous phase[13, 41], and these Ag+ ions are responsible for the antibacterial activity of the materials[30, 42-44]. Compare the antibacterial activity of mSiO$_2$@NH$_2$@Ag and mSiO$_2$@Ag without APTS modification procedure; we could see that APTS modification procedure play a very important role in the immobilization of silver nanoparticles onto mSiO$_2$. Because the amino group of APTS could absorb a larger amount of Ag+ ions tightly through the complex and electrostatic interactions between Ag+ ions and amino functional groups, thus, a larger amount of Ag+ ions were absorbed onto mSiO$_2$ and reduced to Ag nanoparticles through the next ultrasonic wave reaction method. However, there only a small amount of Ag+ ions could be absorbed onto mSiO$_2$ without APTS modification and the created Ag nanoparticles also could easily break away from the channels of mSiO$_2$ without amino functional groups' interactions during the filtration and washing procedure [45](TEM image of mSiO$_2$@Ag find Ag nanoparticles hardly, not shown). So, the mSiO$_2$@Ag without APTS modification procedure has little antibacterial activity.

To further study the antibacterial properties of mSiO$_2$@NH$_2$@Ag samples, the minimum inhibitory concentration (MIC) and minimum bactericidal concentration (MBC) tests against E. coli and SAU by tube dilution methods were also evaluated. A serial of doubling dilution of the mSiO$_2$@NH$_2$@Ag were prepared in the tubes and each dilution was inoculated with the Luria-Bertani (LB) liquid medium in a 1:1 volume ratio, and the final concentration of the mSiO$_2$@NH$_2$@Ag in the tubes were in a range of 0.5-0.0039 mg/mL. Then, 0.2 mL of 10^9 CFU/mL E. coli or 10^8

CFU/mL ASU were added to above LB liquid medium containing different concentrations of mSiO$_2$@NH$_2$@Ag and then incubated at 37 °C for 24 h with continuous agitation (180 rpm). The lowest concentration of mSiO$_2$@NH$_2$@Ag that inhibited the visible growth of colony formation was defined as the MIC. The MBC was determined by subculturing 0.2 mL LB liquid from broth dilution of above MIC tube to LB solid medium plate. After incubation at 37 °C for 24 h, the lowest concentration of the mSiO$_2$@NH$_2$@Ag that does not support colony formation was defined as the MBC. The experiments results showed that the MIC and MBC of mSiO$_2$@NH$_2$@Ag against SAU were 0.156 (the 6[#] tube in Fig.4A, which equal to 5.06 μg/mL of Ag) and 0.3125 mg/mL (Fig.5A, 10.12 μg/mL of Ag), respectively. In the case of E. coli, the MIC and MBC of mSiO$_2$@NH$_2$@Ag were found to be 0.3125 (the 5[#] tube in Fig.4B, 10.12 μg/mL of Ag) and 0.625 mg/mL (Fig.5C, 20.24 μg/mL of Ag). Significant studies showed that the major factor for the MIC and MBC of a material was the interaction of bacteria with active Ag [17, 27, 30], and several studies have reported in the literature involving silver-containing mesoporous silica compounds have shown that the MIC of silver particles for E. coli ranges from 2 to 75 μg/mL of Ag[30, 46]. For example, the MIC values for E. coli obtained for the Ag-SiO$_2$ nanocomposite was 300μg/mL (37.65μg/mL of Ag)[13]; the MIC values for E. coli obtained for the Ag-SiO$_2$ nanocomposite produced by Egger et al. was 62.5 μg/mL (12.5μg/mL of Ag)[46]; the MIC values of AgCl-mesoporous silica (AgCl-SBA-15) and Ag-mesoporous silica nanocomposite (Ag-SBA-15) for E. coli were 25 μg Ag/mL and 100 μg[30] and 203 μg[47] Ag/mL, respectively; the Ag-mesoporous silica

13

nanocomposite (Ag-MCM-41) for E. coli were 258.5 μg Ag/mL[47]. Compared with above-mentioned silver-containing mesoporous silica compounds, the present mSiO$_2$@NH$_2$@Ag exhibited more excellent antibacterial activities according to the Ag contents in the materials. The excellent antibacterial activity of mSiO$_2$@NH$_2$@Ag was due to the mSiO$_2$@NH$_2$@Ag could offer high surface area for the load of a larger amount of silver nanoparticles at the outer channels to improve the antibacterial efficiency, because these open perpendicular nanoporous channels make silver nanoparticles get in touch with bacteria conveniently.

3.3 The reuse study

In order to evaluate the possibility of regeneration and reuse of the mSiO$_2$@NH$_2$@Ag nanocomposites, reuse experiments have been performed. The used mSiO$_2$@NH$_2$@Ag were washed and centrifuged five times with deioned water, and its antibacterial effect was evaluated by IZD test against E. coli and SAU. The result showed that the IZD against SAU and E. coli were still 20 cm and 14 cm, respectively (Fig. 6). For further evaluating the reuse possibility, the successive 5 reuse cycles experiments were performed and found the IZD test against E. coli and and SAU were 15.7 and 11.6 cm in 5th cycle, respectively, the silver content of mSiO$_2$@NH$_2$@Ag after 5 cycles use and washing was 2.68% according the ICP-OES measurement. These showed that mSiO$_2$@NH$_2$@Ag had slow release property and could be used as a recyclable material. Moreover, the stabilization experiment of Ag concentration in 0.05 M Tris–HCl buffer solution (pH 7.4) at 37°C against the immersion time was also studied. As shown in Fig. 7, the release rate of Ag was

relatively high during the initial 16 hours and then stayed almost constant. The slow release property of Ag nanoparticles from the mSiO$_2$ layers was due to the collective coordination effect of large surface area of mSiO$_2$ and the amino functional groups' complex interactions, and this ensure the used mSiO$_2$@NH$_2$@Ag could be reused when it was applied in water pollution problem.

4. Conclusions

In summary, we have synthesized silver nanoparticles-supported surface mesoporous silica nanocomposites for antibacterial applications. The modification of APTS could affect the silver content and antibacterial activity of nanocomposites. The silver nanoparticles were directly created on the surface of mesoporous silica by in stiu chemical reduction of Ag precursor using ultrasonic wave reaction method. The synthesized nanocomposites were examined against both gram-negative E. coli and gram-positive SAU for their antibacterial efficacy. The results demonstrated that the synthesized nanocomposites exhibited more excellent antibacterial properties than those reported silver-containing traditional mesoporous silica compounds. Because of the slow release property of Ag nanoparticles, the synthesized nanocomposites could be used as a recyclable material in various antibacterial applications, such as water purification systems and environmental control of bacteria.

References

1. E. R. Kenawy, S. D. Worley and R. Broughton, *Biomacromolecules*, 2007, **8**, 1359-1384.

2. A. Kumar, P. K. Vemula, P. M. Ajayan and G. John, *Nat. Mater.*, 2008, **7**, 236-241.

3. M. J. Saif, J. Anwar and M. A. Munawar, *Langmuir*, 2009, **25**, 377-379.

4. M. A. Vargas-Reus, K. Memarzadeh, J. Huang, G. G. G. Ren and R. P. Allaker, *Int. J. Antimicrob. Ag*, 2012, **40**, 135-139.

5. R. Bhattacharya and P. Mukherjee, *Adv Drug Deliver. Rev.*, 2008, **60**, 1289-1306.

6. M. V. Liga, E. L. Bryant, V. L. Colvin and Q. L. Li, *Water Res.*, 2011, **45**, 535-544.

7. S. G. Chen, Y. J. Guo, H. Q. Zhong, S. J. Chen, J. A. Li, Z. C. Ge and J. N. Tang, *Chem. Eng. J.*, 2014, **256**, 238-246.

8. J. P. Ruparelia, A. K. Chatteriee, S. P. Duttagupta and S. Mukherji, *Acta Biomater.*, 2008, **4**, 707-716.

9. T. Jin and Y. P. He, *J. Nanopart. Res.*, 2011, **13**, 6877-6885.

10. J. Pasquet, Y. Chevalier, E. Couval, D. Bouvier, G. Noizet, C. Morliere and M. A.

Bolzinger, *Int. J. Pharmaceut.*, 2014, **460**, 92-100.

11. M. Eshed, J. Lellouche, A. Gedanken and E. Banin, *Adv. Funct. Mater.*, 2014, **24**,

1382-1390.

12. S. K. Rastogi, V. J. Rutledge, C. Gibson, D. A. Newcombe, J. R. Branen and A. L.

Branen, *Nanomed-Nanotechnol.*, 2011, **7**, 305-314.

13. Y. H. Kim, D. K. Lee, H. G. Cha, C. W. Kim and Y. S. Kang, *J. Phys. Chem. C*,

2007, **111**, 3629-3635.

14. F. A. Sheikh, H. W. Ju, B. M. Moon, H. J. Park, J. H. Kim, O. J. Lee and C. H.

Park, *J. Biomed. Mater. Res. A*, 2014, **102**, 3459-3469.

15. M. Saleem, M. Nazir, M. S. Ali, H. Hussain, Y. S. Lee, N. Riaz and A. Jabbar, *Nat.*

Prod. Rep., 2010, **27**, 238-254.

16. W. G. I. U. Rathnayake, H. Ismail, A. Baharin, I. M. C. C. D. Bandara and S.

Rajapakse, *J. Appl. Polym. Sci.*, 2014, **131**.

17. C. Marambio-Jones and E. M. V. Hoek, *J. Nanopart. Res.*, 2010, **12**, 1531-1551.

18. J. R. Morones, J. L. Elechiguerra, A. Camacho, K. Holt, J. B. Kouri, J. T. Ramirez

and M. J. Yacaman, *Nanotechnology*, 2005, **16**, 2346-2353.

19. P. Li, J. Li, C. Z. Wu, Q. S. Wu and J. Li, *Nanotechnology*, 2005, **16**, 1912-1917.

20. M. Singh, S. Singh, S. Prasad and I. S. Gambhir, *Dig. J. Nanomater. Bios.*, 2008,

3, 115-122.

21. A. Top and S. Ulku, *Appl.Clay Sci.*, 2004, **27**, 13-19.

22. B. Kwakye-Awuah, I. Radecka, M. A. Kenward and C. D. Williams, *J. Chem.*

Technol. Biot., 2008, **83**, 1255-1260.

23. B. Kwakye-Awuah, C. Williams, M. A. Kenward and I. Radecka, *J. Appl. Microbiol.*, 2008, **104**, 1516-1524.

24. E. Abdullayev, K. Sakakibara, K. Okamoto, W. B. Wei, K. Ariga and Y. Lvov, *Acs Appl. Mater. Inter.*, 2011, **3**, 4040-4046.

25. J. S. Lee and W. L. Murphy, *Adv. Mater.*, 2013, **25**, 1173-1179.

26. H. S. Jia, W. S. Hou, L. Q. Wei, B. S. Xu and X. G. Liu, *Dent. Mater.*, 2008, **24**, 244-249.

27. H. Yang, Y. Liu, Q. H. Shen, L. F. Chen, W. H. You, X. M. Wang and J. S. Sheng, *J .Mater. Chem.*, 2012, **22**, 24132-24138.

28. D. Carmona, P. Lalueza, F. Balas, M. Arruebo and J. Santamaria, *Micropor. Mesopor. Mat.*, 2012, **161**, 84-90.

29. D. V. Quang, P. B. Sarawade, A. Hilonga, J. K. Kim, Y. G. Chai, S. H. Kim, J. Y. Ryu and H. T. Kim, *Colloid Surface A*, 2011, **389**, 118-126.

30. B. Naik, V. Desai, M. Kowshik, V. S. Prasad, G. F. Fernando and N. N. Ghosh, *Particuology*, 2011, **9**, 243-247.

31. Y. I. Seo, Y. J. Lee, D. G. Kim, K. H. Lee and Y. Do Kim, *Micropor. Mesopor. Mat.*, 2011, **139**, 211-215.

32. L. H. Dong, T. Liu, L. Zhang and Y. S. Yin, *Appl. Chem.Eng., Pts 1-3*, 2011, **236-238**, 1775-1778.

33. Y. Deng, D. Qi, C. Deng, X. Zhang and D. Zhao, *J. Am. Chem. Soc.*, 2008, **130**, 28-31.

34. S. B. Yoon, J. Y. Kim, J. H. Kim, Y. J. Park, K. R. Yoon, S. K. Park and J. S. Yu, *J. Mater. Chem.*, 2007, **17**, 1758-1761.

35. X. C. Fu, J. Wu, C. G. Xie, Y. Zhong and J. H. Liu, *Anal. Methods-Uk*, 2013, **5**, 2615-2622.

36. X. C. Fu, X. Chen, J. Wang, J. H. Liu and X. J. Huang, *Electrochim. Acta*, 2010, **56**, 102-107.

37. X. L. Li, W. W. Zuo, M. Luo, Z. S. Shi, Z. C. Cui and S. Zhu, *Chem. Res. Chin.Univ.*, 2013, **29**, 1214-1218.

38. H. L. Li, N. Perkas, Q. L. Li, Y. Gofer, Y. Koltypin and A. Gedanken, *Langmuir*, 2003, **19**, 10409-10413.

39. M. S. Zhu, P. L. Chen and M. H. Liu, *Acs Nano*, 2011, **5**, 4529-4536.

40. L. S. Zhang, K. H. Wong, Z. G. Chen, J. C. Yu, J. C. Zhao, C. Hu, C. Y. Chan and P. K. Wong, *Appl. Catal. a-Gen.*, 2009, **363**, 221-229.

41. T. Liu, X. Song, Z. W. Guo, Y. H. Dong, N. Guo and X. T. Chang, *Colloid Surface B*, 2014, **116**, 793-796.

42. S. H. Min, J. H. Yang, J. Y. Kim and Y. U. Kwon, *Micropor. Mesopor. Mat.*, 2010, **128**, 19-25.

43. H. Yang, W. H. You, Q. H. Shen, X. M. Wang, J. S. Sheng, D. Cheng, X. D. Cao and C. C. Wu, *Rsc Adv.*, 2014, **4**, 2793-2796.

44. W. K. Jung, H. C. Koo, K. W. Kim, S. Shin, S. H. Kim and Y. H. Park, *Appl. Environ. Microb.*, 2008, **74**, 2171-2178.

45. Q. Shen, J. Wang, H. Yang, X. Ding, Z. Luo, H. Wang, C. Pan, J. Sheng and D.

Cheng, *J. Non-Cryst. Solids*, 2014, **391**, 112-116.

46. S. Egger, R. P. Lehmann, M. J. Height, M. J. Loessner and M. Schuppler, *Appl. Environ. Microb.*, 2009, **75**, 2973-2976.

47. A. Szegedi, M. Popova, K. Yoncheva, J. Makk, J. Mihaly and P. Shestakova, *J. Mater. Chem. B*, 2014, **2**, 6283-6292.

Figure Captions:

Fig. 1. (A) Schematic illustration of procedures for preparation of mSiO$_2$@NH$_2$@Ag. (B) SEM image of mSiO$_2$ microspheres. (C) SEM image of mSiO$_2$@NH$_2$@Ag, the inset show the low magnification and high magnification TEM images of mSiO$_2$@NH$_2$@Ag, respectively.

Fig. 2. (A) FT-IR spectra of (a) mSiO$_2$, (b) mSiO$_2$@NH$_2$ and (c) mSiO$_2$@NH$_2$@Ag. (B) XPS spectra of (a) (a) mSiO$_2$, (b) mSiO$_2$@NH$_2$ and (c) mSiO$_2$@NH$_2$@Ag, insert is the high resolution Ag3d XPS spectra of mSiO$_2$@NH$_2$@Ag. (C) Room-temperature XRD patterns of (a) mSiO$_2$ and (b) mSiO$_2$@NH$_2$@Ag.

Fig. 3. The inhibition zones test results of mSiO$_2$, mSiO$_2$@NH$_2$ and mSiO$_2$@NH$_2$@AgNPs against (A) SAU (10^8 CFU) and (B) E. coli (10^9 CFU).

Fig. 4. The MIC experiment results of mSiO$_2$@NH$_2$@Ag at different concentrations against (A) SAU (10^8 CFU) and (B) E. coli (10^9 CFU) by tube dilution method. The concentrations of mSiO$_2$@NH$_2$@Ag from 1 to 9 tubes were 0.5, 0.25, 0.125, 0.0625, 0.03125, 0.0156, 0.0078, 0.0039 and 0 mg/mL, respectively.

Fig. 5. The MBC experiment results of mSiO$_2$@NH$_2$@Ag against (A, B) SAU (10^8 CFU) and (C, D) E. coli (10^9 CFU). The concentrations of mSiO$_2$@NH$_2$@Ag from A

to D plates were 0.03125, 0.0156, 0.0625 and 0.03125 mg/mL, respectively.

Fig.6. Inhibition zones test results of the used $mSiO_2@NH_2@Ag$ against (A) SAU
(10^8 CFU) and (B) E. coli (10^9 CFU). Before test, the used $mSiO_2@NH_2@Ag$ were
washed and centrifuged five times with deioned water.

Fig. 7. Ag+ release from $mSiO_2@NH_2@Ag$ into Tris–HCl solution (pH 7.4) at 37°C
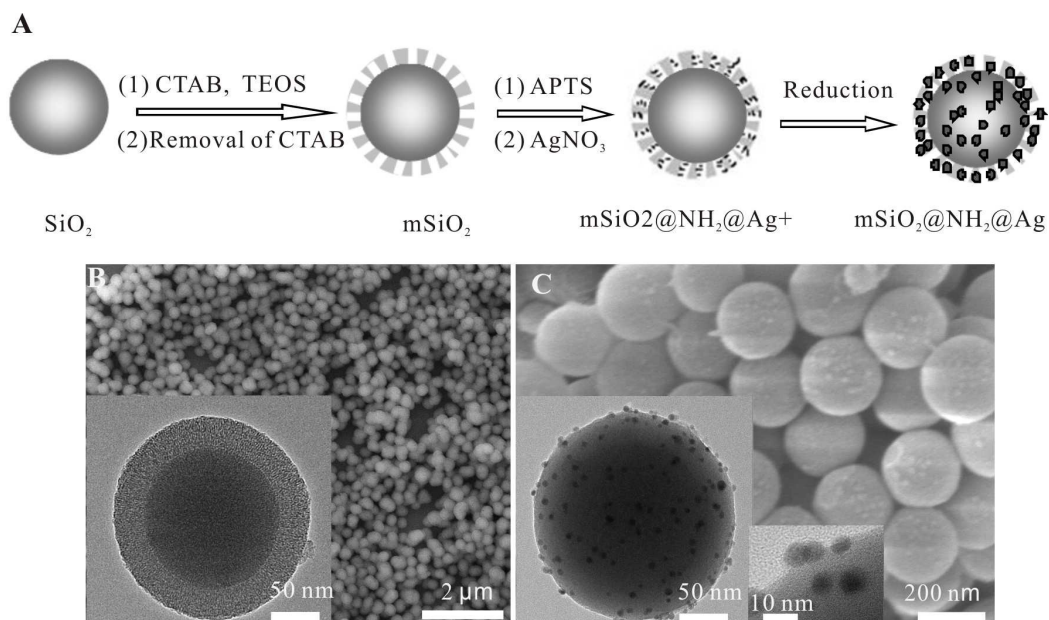against immersion time.

Fig. 1. (A) Schematic illustration of procedures for preparation of mSiO$_2$@NH$_2$@Ag.

(B) SEM image of mSiO$_2$ microspheres. (C) SEM image of mSiO$_2$@NH$_2$@Ag, the

inset show the low magnification and high magnification TEM images of

mSiO$_2$@NH$_2$@Ag, respectively.

Fig. 2. (A) FT-IR spectra of (a) mSiO$_2$, (b) mSiO$_2$@NH$_2$ and (c) mSiO$_2$@NH$_2$@Ag.

(B) XPS spectra of (a) (a) mSiO$_2$, (b) mSiO$_2$@NH$_2$ and (c) mSiO$_2$@NH$_2$@Ag, insert

is the high resolution Ag3d XPS spectra of mSiO$_2$@NH$_2$@Ag. (C) Room-temperature

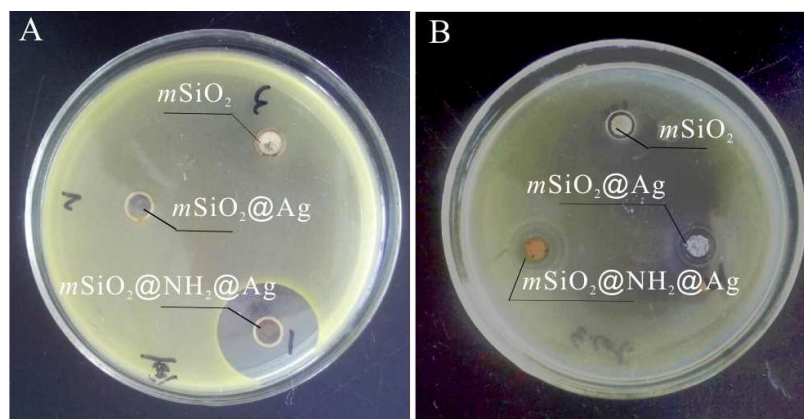XRD patterns of (a) mSiO$_2$ and (b) mSiO$_2$@NH$_2$@Ag.

Fig. 3. The inhibition zones test results of mSiO$_2$, mSiO$_2$@NH$_2$ and mSiO$_2$@NH$_2$@AgNPs against (A) SAU (10^8 CFU) and (B) E. coli (10^9 CFU).
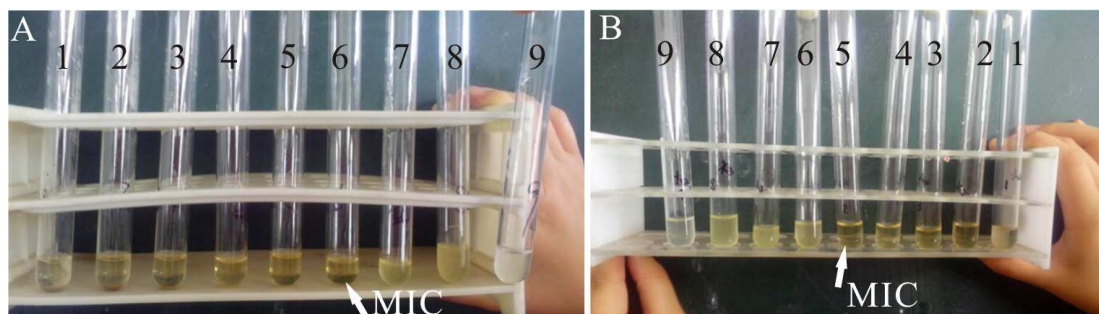
Fig. 4. The MIC experiment results of mSiO$_2$@NH$_2$@Ag at different concentrations against (A) SAU (10^8 CFU) and (B) E. coli (10^9 CFU) by tube dilution method. The concentrations of mSiO$_2$@NH$_2$@Ag from 1 to 9 tubes were 0.5, 0.25, 0.125, 0.0625, 0.03125, 0.0156, 0.0078, 0.0039 and 0 mg/mL, respectively.
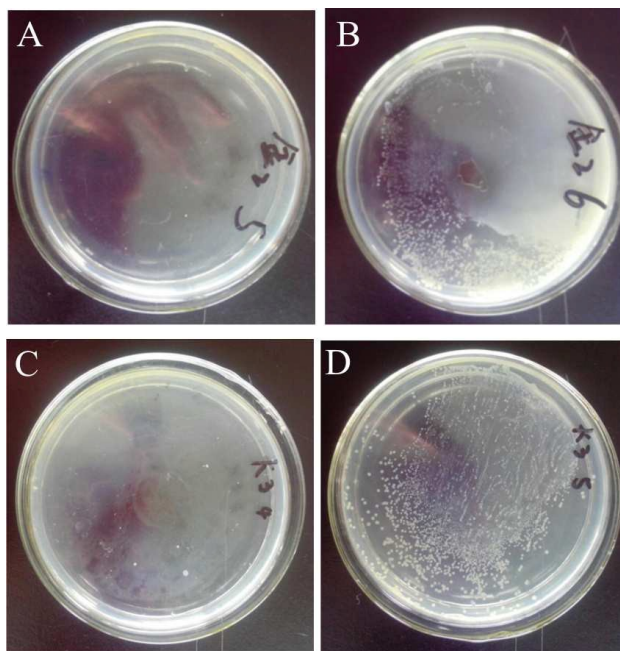
Fig. 5. The MBC experiment results of mSiO$_2$@NH$_2$@Ag against (A, B) SAU (10^8 CFU) and (C, D) E. coli (10^9 CFU). The concentrations of mSiO$_2$@NH$_2$@Ag from A to D plates were 0.03125, 0.0156, 0.0625 and 0.03125 mg/mL, respectively.
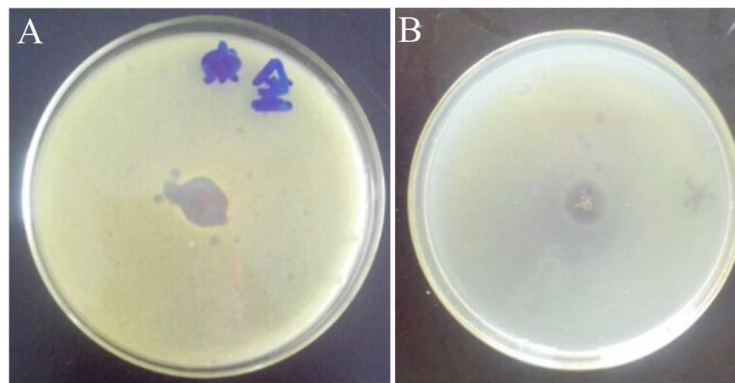
Fig. 6. Inhibition zones test results of the used mSiO$_2$@NH$_2$@Ag against SAU (A, 10^8 CFU) and E. coli (B, 10^8 CFU). Before test, the used mSiO$_2$@NH$_2$@Ag were washed and centrifuged five times with deioned water.
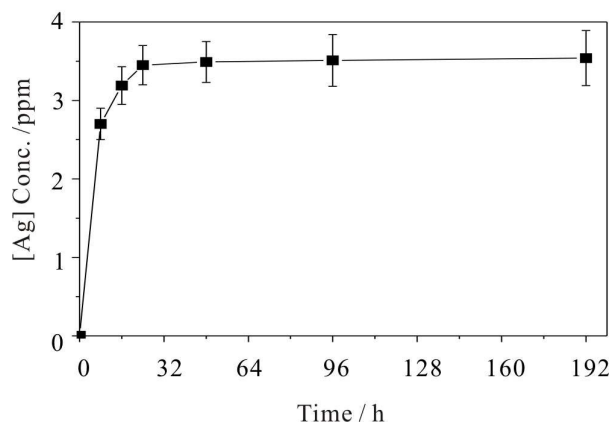
Fig.7. Ag+ release from *m*SiO$_2$@NH$_2$@Ag into Tris–HCl solution (pH 7.4) at 37°C against immersion time.

A

SiO₂   mSiO₂   mSiO2@NH₂@Ag+   mSiO₂@NH₂@Ag